LOSS IN VERTICAL-CAVITY SOURCE-EMITTING LASERS AS A RESULT OF IMPURITIES

By

Charlene Tai

Senior Thesis in Electrical and Computer Engineering

University of Illinois at Urbana-Champaign

Advisor: Kent D. Choquette

December 2014

Abstract

Vertical-cavity source emitting lasers (VCSELs) are useful for optical communication light sources because of their low cost and operating power. An understanding of the cavity optical loss is necessary in order to best optimize the design and performance of the devices. Using a method which measures the sub-threshold emission spectra, the loss can be quantitatively calculated. With this, optical loss of VCSELs with varying doping levels can be evaluated. With a semiconductor parameter analyzer, light output power as a function of injection current is measured for each different set of VCSELs to find the threshold current. The resulting current density can be found for each laser mesa size and the point where the loss becomes independent of the aperture size can be identified. Using an optical spectrum analyzer, the spectral separation between the cold-cavity fundamental mode and the first higher-order mode can then be found without thermal effects by measuring the spectral splitting for each VCSEL biased at an injection current of approximately 0.9 times the threshold. The spectral splitting of small diameter lasers can be used to calculate the optical loss using the Helmholtz wave equation with an imaginary refractive index. The field amplitude loss can be extracted from the imaginary part of the resulting wavenumbers. Two VCSEL samples with different doping are measured in this study. The calculated size-dependent loss is found to be the same for the two samples and thus it seems that that effects of the different doping are not sufficient to affect the cavity loss. It is, however, clearly shown that the introduction of impurities to create a doped pn junction does indeed create optical loss.

Subject Keywords: vertical cavity surface emitting laser; semiconductor laser; optical loss; oxide-confined micro-cavity

Acknowledgments

The following work would not have been possible without the aid and contributions of a number of people. First and foremost, I would like to thank my advisor, Professor Kent D. Choquette, for all the support and advice he has given and the opportunities he has help made available to me. His counsel, patience, and enthusiasm has been a great motivator and has made it possible for me to get the most out of the past few terms. I am also extremely grateful to Stewart Fryslie and Captain Janice Blane for all the help I've received from them, ranging from general knowledge and advice to little tips and tricks for when taking measurements and running the procedures. I would like to also thank Bradley Thompson and Gautham Ragunathan for the two samples they fabricated that I used in this work.

Contents

1. Introduction

1.1 Motivation

Vertical cavity surface emitting lasers (VCSELs) are a type of semiconductor laser that emits perpendicular to the semiconductor wafer surface as opposed to edge emitting lasers, which emit parallel from the wafer edge. Advantages of VCSELs include a variety of their characteristics such as small cavity volume, high mirror reflectivity and modulation bandwidth, as well as low power consumption. VCSELs can also be tested throughout the production process to better control the quality of the devices. Additionally tens of thousands of devices can be fabricated simultaneously in arrays from a single wafer because of their small sizes [1].

VCSELs have become increasingly important in a number of technologies with applications in various fields including data communications, infrared illumination and heating, printing, and optical sensing. They are used in many computer communication applications such as optical interconnects in data centers that nowadays can span kilometers in length. Increasing demand for performance requirements has resulted in a need for design optimization and further research for improving micro-cavity lasers. Driven by the ever-increasing performance requirements, higher data transmission bandwidth are required while simultaneously still maintaining lower power consumption and narrow spectral width. These demands tend to encourage development in small diameter oxide-confined VCSELs. For small cavity VCSELs it has been found that their performance can sometimes depend on their cavity diameter, particularly for relatively small (≤ 8 micron) diameters. In this study, we will study the size-dependency of optical loss as well as the effect of doping levels.

1.2 Technical Background

The structure of a VCSEL consists of distributed Bragg reflector (DBR) layers sandwiching an active region that is composed of a few quantum wells and can be designed for top emission through a ring contact, as sketched in Figure 1, or bottom emission through a transparent substrate. It has been demonstrated that through selective oxidation, optical losses in the cavity can be reduced [2], [3]. The DBR layers form the cavity mirrors that provide optical feedback to the system: they consist of alternating layers of low and high refractive indices at quarter wavelength thicknesses, resulting in extremely high mirror reflectivity. Just like all lasers, the optical gain must overcome the mirror loss and absorption losses within the cavity to begin lasing operation. Threshold gain γ_{th} is often represented as

$$\gamma_{th} = \alpha - \frac{1}{2L}\ln(R_1 R_2) \tag{1.1}$$

where α is the cavity loss, L is the cavity length, and R_1 and R_2 are the reflectivity of the DBR mirrors. The second term in Eq. 1.1 encompasses the mirror loss while the first term, the cavity loss, can be decomposed into a size-dependent value plus a constant. There is evidence that this size-dependent optical loss is prominent in small diameter oxide-confined VCSELs and exhibit properties that do not linearly relate to the device size [1], [4], [5].

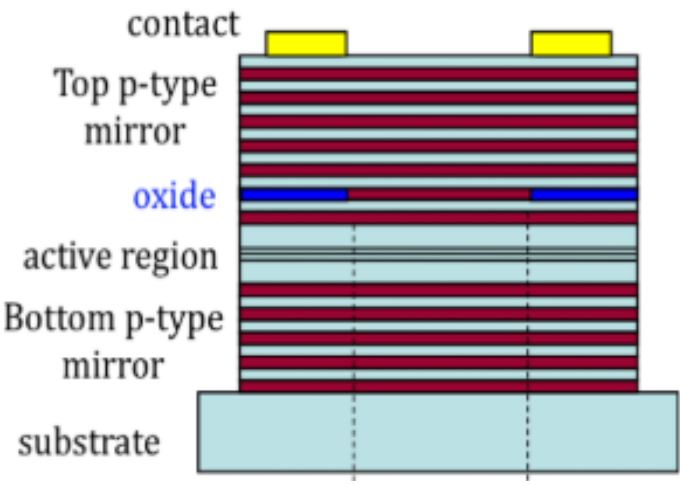

Figure 1 Side view of general structure of a VCSEL.

2. Literature Review

Many laser applications desire an output beam that has a single-transverse-mode; however VCSELs tend to operate in a multitude of transverse modes. As a result, various methods of mode confinement have been demonstrated such as oxide apertures [6], proton-implanted apertures [7], oxide/implant hybrid structures [8], surface relief etched lasers [9], photonic crystal patterns [10]–[15], and etched holey patterns [16]. For the photonic crystal VCSEL structures, it has been demonstrated that single-mode operation can be a result of loss to higher-order modes [17].

Size-dependent optical loss has been determined in the past by analyzing the external quantum efficiency [18], [19] or threshold voltage [1], approaches in which thermal effects will influence optical scattering loss. A method to calculate the effect of loss in photonic crystal VCSELs on the transverse confinement has been developed through incorporating a complex index for the surrounding clad [20] region around the laser cavity, using simple cylindrical waveguide analysis and sub-threshold spectral characterization [21]. This method has also been applied to oxide-confined VCSELs [22].

The laser modes can be determined from solutions to the Helmholtz equation [21]

$$\nabla^2 U(r,\phi,z) + n^2(r){k^2}_0 U(r,\phi,z) = 0 \tag{2.1}$$

where U is the field profile, n is the refractive index profile, k_0 is the wavenumber. Solutions to this model assuming a cylindrical waveguide is

$$U(r,\phi,z) = u(r)e^{-im\phi}e^{-i\beta z} \tag{2.2}$$

where m is an integer and β is the propagation constance given by $2\pi/L$, where L is the longitudinal cavity length. Combing (2.1) and (2.2) and using a finite-difference approach, and fitting the results to the experimental data, gives an eigenvalue expressed as

$$\left[\frac{u_{j+1} - 2u_j + u_{j-1}}{(\Delta r)^2} + \frac{1}{r_j}\frac{u_{j+1} - u_{j-1}}{2\Delta r} - \left(\beta^2 + \frac{m^2}{r^2}\right)u_j\right] = -{n_j}^2{k_0}^2 u_j \tag{2.3}$$

where j is an index associated with a point in space. The core and cladding refractive indices determine the solution to (2.3) so the inclusion of a complex refractive index implies that the field eigenvector and wavenumber will also be complex. The resonant wavelength λ_0 can be found from the wavenumber by $\lambda_0 = 2\pi/Re\{k_0\}$ and the field amplitude loss, α_i, can be extracted by $\alpha_i = Im\{k_0\}$.

The real values of the refractive indices of the core and clad can be calculated from the transmission matrix method [23] using the epitaxial structure and can be used to solve for the fundamental and first

higher-order modes λ_{01} and λ_{11} respectively. We next use experimental data matched to our simulation to find the size-dependent optical loss. The technique we use is to add an imaginary term in the complex cladding which results in mode resonances with greater spectral splitting that matches the measured experimental data. This imaginary component will be proportional to the size-dependent optical loss that arises for small diameter VCSELs.

3. Experimental Method

This section will describe the experimental procedure followed to determine the optical loss of the VCSEL samples. Pictured in Figure 2 is the experimental setup for taking light vs. current measurements as well as spectral measurements. On the left side in Fig. 2 is the ALESSI Probe Station equipped with a camera, fiber probe, photo-detector, and electrical probe. The rack on the right contains the semiconductor parameter analyzer (SPA), optical spectrum analyzer (OSA) and a Keithley current source. For each sample, a set of LIVs and spectra were measured with the SPA and OSA, respectively. A Helmholtz equation solver is then used to quantitatively find the intrinsic loss by comparing calculated spectral splitting between the fundamental mode and the first higher-order mode to values measured from the VCSEL samples with varying mesa size. The two VCSEL samples used in this study are EMC 1005 with a high doping level, and EMC 1006 with a low doping level.

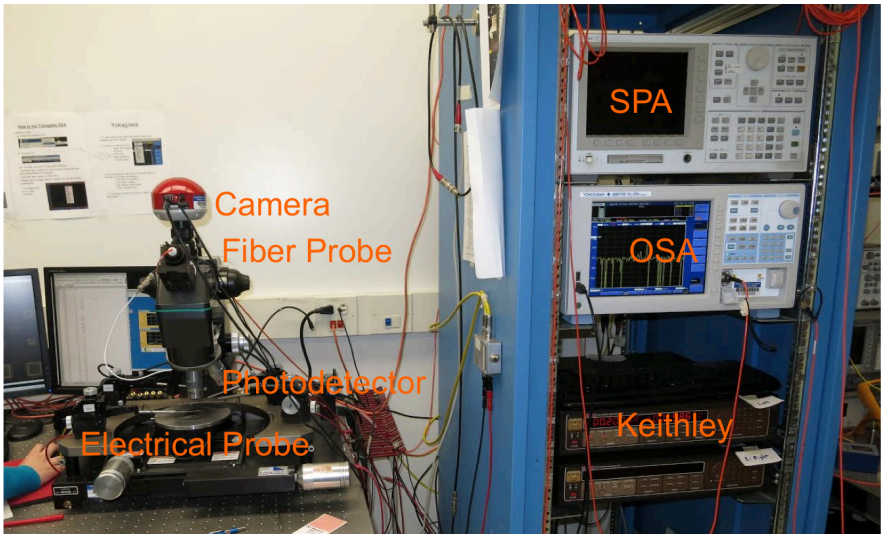

Figure 2 Setup for taking LIV and spectral measurements. Variable current is injected into the devices with the current source; measurements were done with the room lights off to minimize noise when finding spectra.

3.1 Quick VCSEL Measurements

Pictures of one of the tested samples and the probe station are shown in Figure 3 and 4. The unit cell of the mask layout of the tested VCSELs has devices with mesa sizes varying from 30 x 30 µm to 75 x 75 µm in steps of 0.5 or 1 µm, as shown in Fig. 5. The bottom-right corner has the smallest device; the side length increases by 0.5 µm moving along the row to the left, with the largest mesa in the row having a side length of 36.5 µm. The next row up, moving in the reverse direction from left to right, continues with increasing mesa sizes by 0.5 µm until the far end with a 43.5 x 43.5 µm mesa. This pattern continues for the upper two rows,

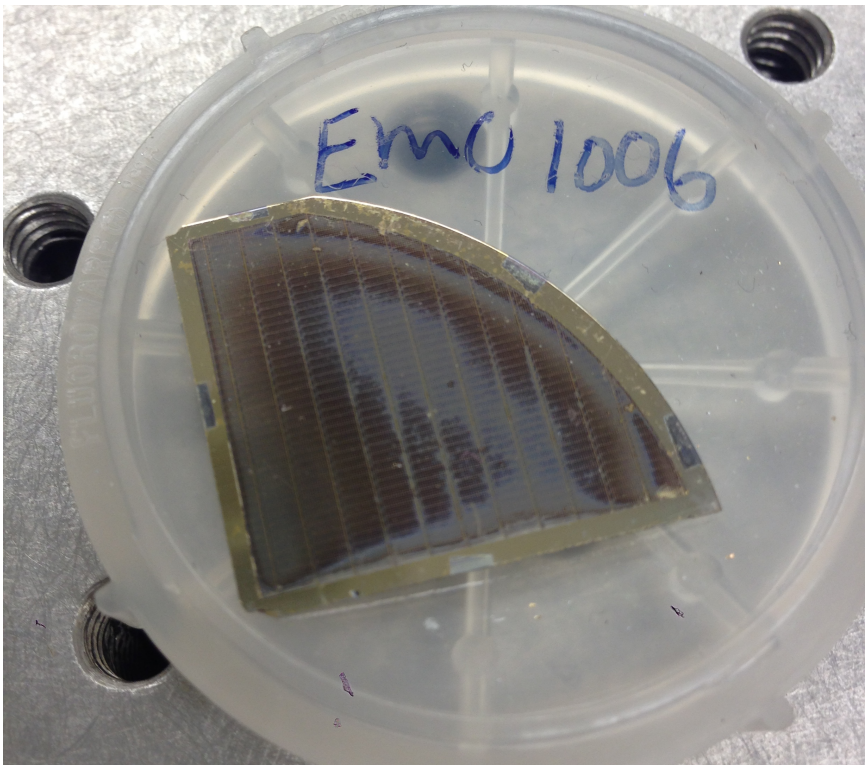

Figure 3 Photo of sample with low doping. Each sample contains hundreds of cells with the mask layout.

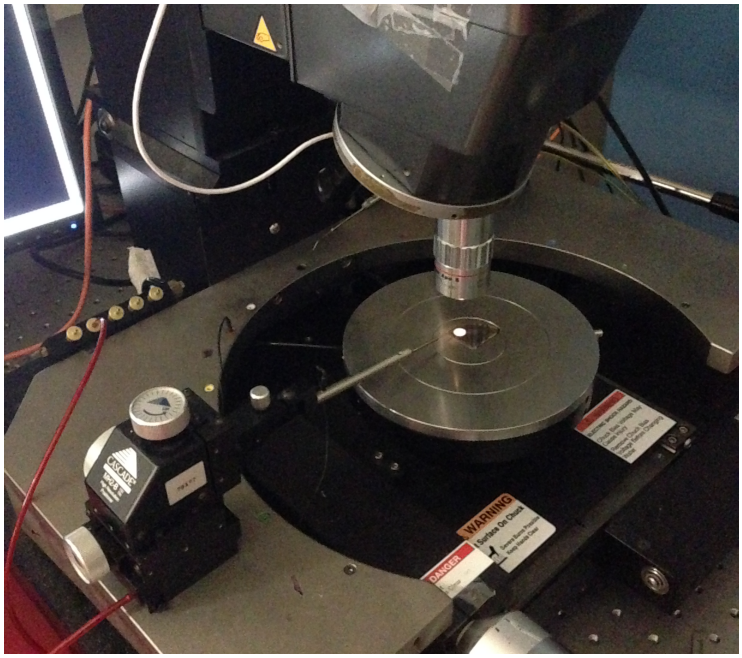

Figure 4 Photo of a sample on ALESSI Probe Station.

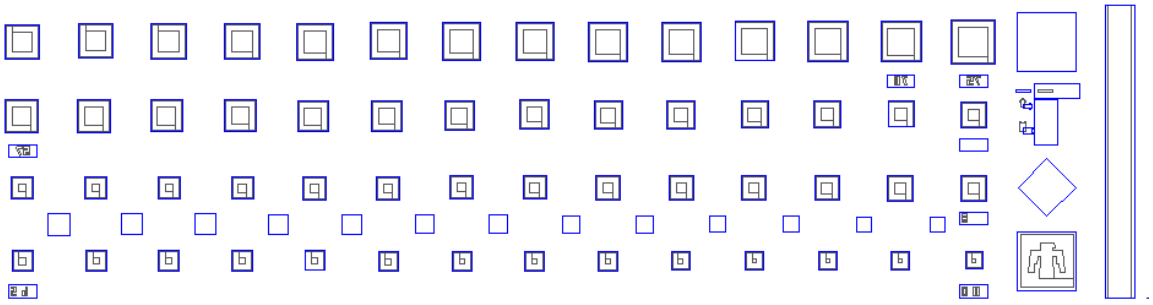

Figure 5 Mask layout of VCSEL wafer fabricated at University of Illinois: Urbana-Champaign.

except instead the mesa side lengths increase by steps of 1 µm. In this manner, VCSELs with a range of aperture sizes, varying by 0.5 or 1.0 micron, can be obtained. The anode contacts for the diode lasers are metal contact rings on the top of the mesa; the back of the wafer acts as the cathode contact.

The oxide aperture size can be determined with a device's electrical conductivity. During fabrication, smaller mesas can be completely oxidized and will result in an open circuit when current injection is attempted. However, as larger mesas are measured, for some mesa size there will be current conduction; the first mesa to conduct will thus have an aperture size of 0.5 ≤ 1 µm depending on whether it is in the lower or upper two rows of the unit cell, respectively.

To begin measuring the light vs. current characteristics for each device, the largest mesa that is "pinched off," i.e. produces an open circuit, is found. The next larger mesa that conducts has the smallest diameter cavity as described in the previous paragraph. For the samples used in this study, EMC 1005 was found to have an aperture size of 0.5 µm at the 34 x 34 µm mesa; for EMC 1006, 0.5 µm at the 33.5 x 33.5 µm mesa.

Starting from the VCSEL with an aperture size of approximately a 10 µm, and then moving to smaller mesas, the electrical probe was placed onto the metal contacts and light versus current and voltage (LIVs) curves were measured with the SPA for current injection up to the maximum output power (power rollover, see Fig 6). Injecting greater current could result in damaging the VCSEL. The light-current curve has a constant slope above threshold, as is common for laser diodes, but then shows a characteristic rollover for higher currents due to internal heating.

The LIV characteristics can provide useful information about the device such as the threshold current, rollover current, slope efficiency, and maximum power. Graphically, threshold current is easy to find. It is the point at which stimulated emission overcomes the spontaneous emission and the device begins to

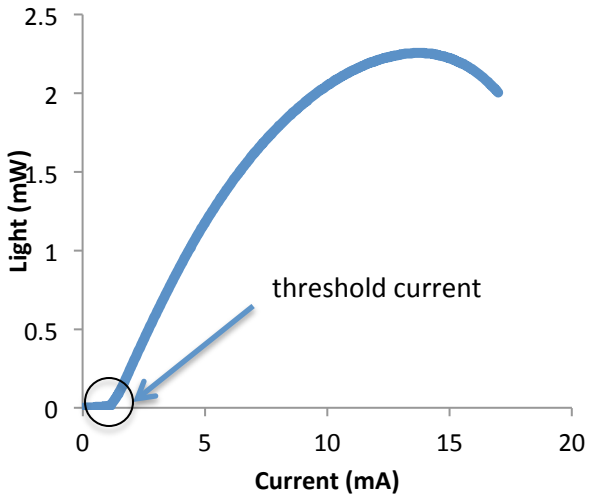

Figure 6 Light vs. current characterization.

lase. It can be often found for smaller aperture VCSELs that the, current threshold is nonexistent indicating that the devices do not lase: they are just light-emitting-diodes.

The threshold current density is found by dividing the threshold current by the aperture size. This is plotted for the two samples in Fig. 7.

For large apertures, there is little or no size-dependence and can be seen by the approximately linear trend. This however is not the case for smaller apertures because scattering loss and current leakage is significant enough to effect lasing characteristics to create significantly higher current density for the smallest VCSELs.

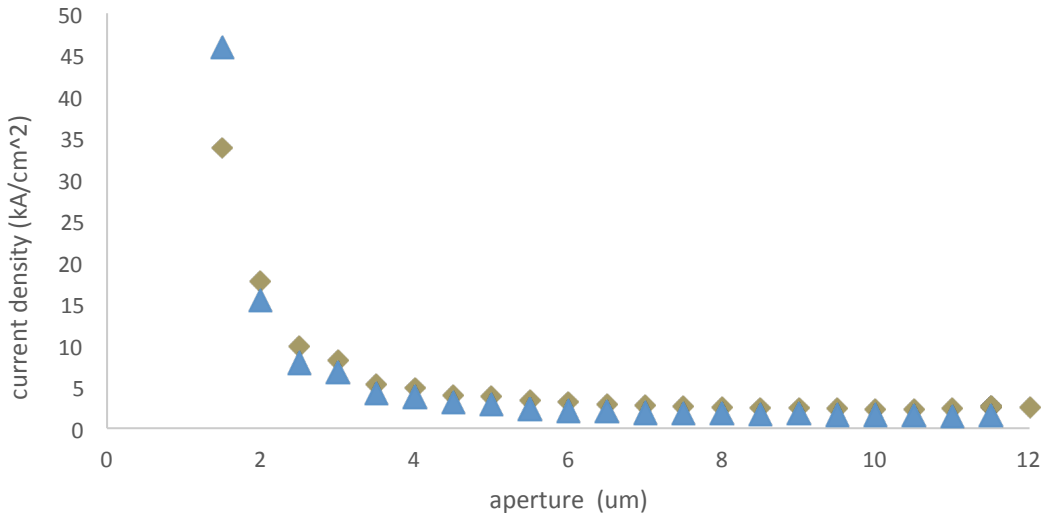

Figure 7 Current density of the two difference samples plotted as a function of aperture size

3.2 Spectral Analysis

For VCSELs with relatively small aperture size (less than approximately 8 micron) , the excess fundamental loss can be quantitatively extracted by examining the spectral difference between the peak wavelength of the fundamental mode and first higher-order mode. To find these, the splitting is first determined using the OSA (Fig. 8).

Measurements of the size-dependent optical loss have been demonstrated using procedures that require lasing [1], [18], [19], but these measurements can be distorted by thermal effects. This can be overcome by measuring the spectral-characterization under the so called "cold-cavity" conditions, meaning at injection currents less than the threshold current. Combined with a Helmholtz waveguide model with circular geometry and incorporating a complex refractive index for the cladding, optical loss in photonic crystal VCSELs [21] and oxide-confined VCSELs [22] has been previously characterized.

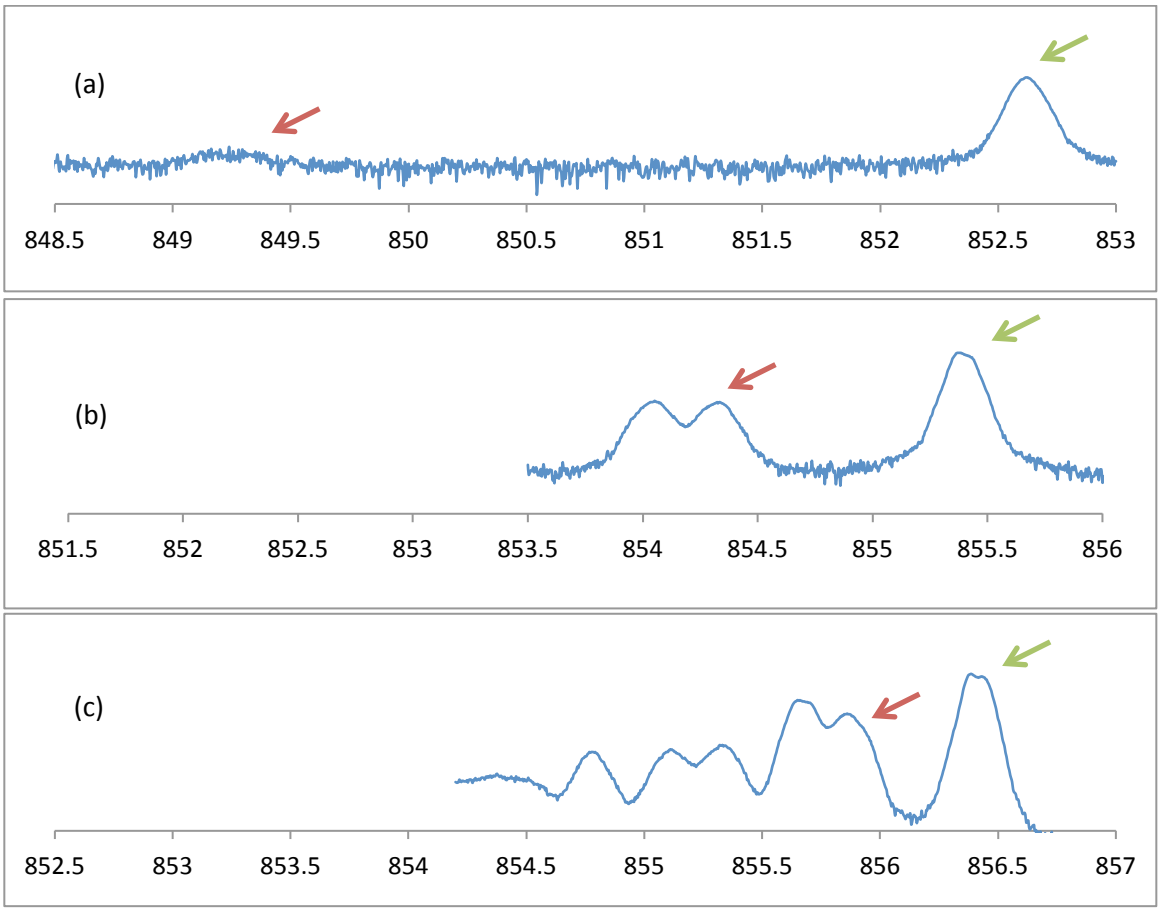

Figure 8 Spectral measurements for the (a) 2 µm, (b) 4 µm, and (c) 6 µm VCSELs from the EMC 1005 sample; the fundamental modes and first higher-order modes are pointed out in green and red arrows, respectively.

Cold-cavity measurements are taken at about 80% of the threshold current for each device size. However, because of imperfect processing, the dimensions of the mesa apertures are not always perfectly square. In the cases where the two dimensions differ, the wavelength degeneracy is lifted, the individual higher-order modes can separate and could be mistaken for multiple modes, such as for the first higher-order mode of Fig. 8c. To avoid this potential confusion, the peak wavelength of each mode is plotted as a function of injection current as shown in Fig. 9. Insuring that the OSA wavelength range is large enough to span multiple VCSEL modes, the spectrum of each device was taken at multiple current injections: a value below threshold and then at least five different injections ranging from threshold to rollover current. By plotting each of the peaks, it is a simple matter to discern which values are actual modes and which are a mode that has been split into two. Modes shift due to thermal heating arising from I^2R heating, and the resulting curves follow a pattern that is not quite quadratic but not quite linear as seen in Figure 9. Separated modes can be determined by irregularities in the curves. The rectangular shape of the aperture causes the mode to separate into two peaks and, when averaged and plotted as a single point, should follow the expected pattern of the transverse modes.

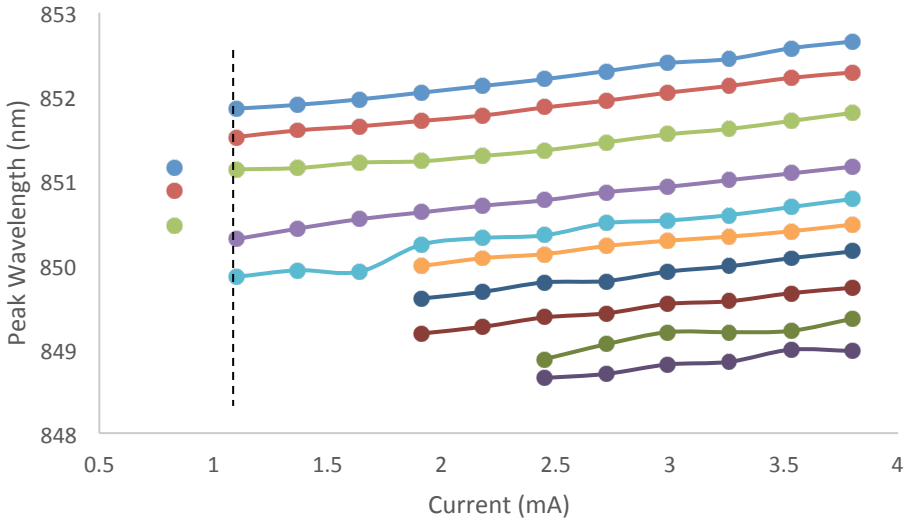

Figure 9 Modal characterizations; modes shift to higher wavelengths at higher currents.

After determining the fundamental and first higher-order mode, the splitting can be found by calculating the difference in the two wavelengths. Fig. 10 shows the measured spectral splitting measured from the two VCSEL samples. Comparing the values of the splitting between the fundamental and first higher-order mode, it is shown that there is no significant difference between the splitting for the two samples.

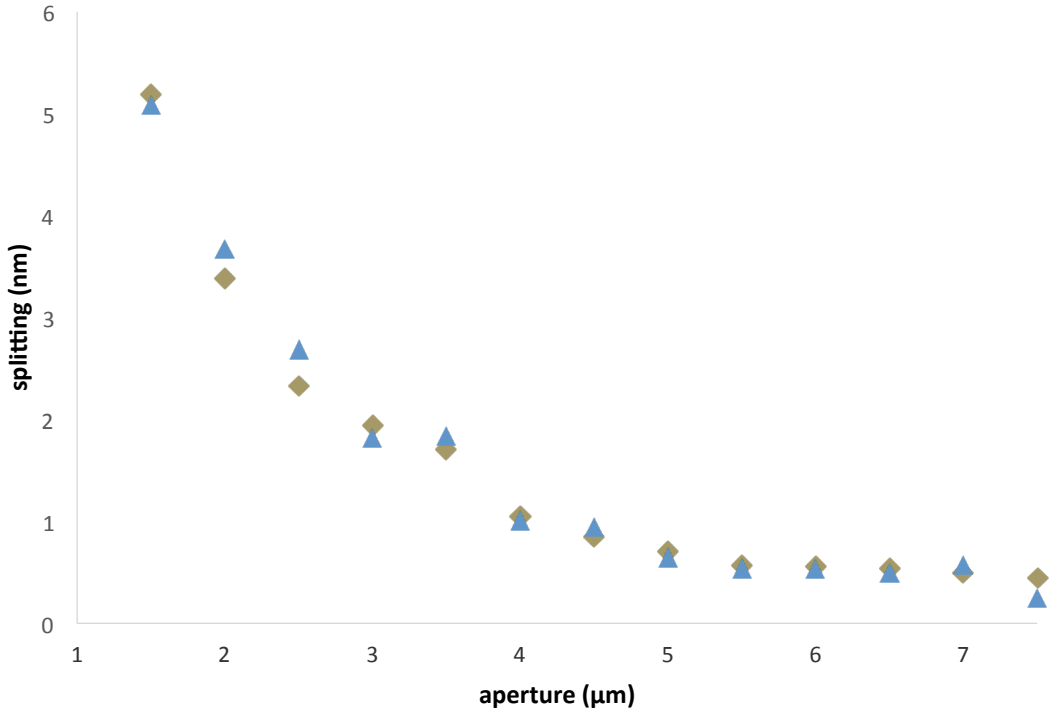

Figure 10 Measured splitting of the two samples with different doping levels.

3.3 Loss Calculations

We next use a method previously used to characterize optical loss in photonic crystal VCSELs [21] and oxide-confined VCSELs [22].

3.3.1 Code Description

The original loss analysis program was designed to be an automated program that uses as input the VCSEL epitaxial structure, photonic crystal parameters, and cavity resonance wavelength as inputs and calculates the effective indices and cavity loss [21]. It has been modified slightly to suit oxide-confined VCSELs [22]. The program works by matching the measured values of spectral splitting with calculated ones. Given information about the epitaxial structure, the refractive index of the core and of the surrounding clad can be determined. The program calculations are most sensitive to the difference between the refractive indices rather than the absolute values of the indices, reducing the effect of uncertainties pertaining to the refractive index values used in the program.

By solving the wave equation in a cylindrical geometry, the program calculates an initial value of splitting assuming that there is no loss then it iteratively adjusts the value of the imaginary part of the clad until it is able to match the measured splitting. Note for sufficiently large diameter, the calculated spectral

splitting matches the measurements; however for smaller diameter, the addition of imaginary refractive index accounts for the higher optical loss.

3.3.2 Implementation

Because the code was adapted from a program originally designed for photonic crystals, a few adjustments were made to better suit the needs of oxide-confined VCSEL samples, as noted in Appendix A. The epitaxial structure input file was first changed to properly reflect the two samples that are studied. Additionally the measured splitting $\Delta\lambda$ was input as the difference between the fundamental mode and the first higher-order mode. The refractive index of the core n_c is calculated using

$$\Delta\lambda = \frac{\sqrt{n_c - n_s}}{\sqrt{2n_c}\pi}\frac{\lambda^2}{n_c a} \tag{3.1}$$

where λ is the wavelength of the fundamental mode, n_s is the refractive index surrounding clad, and a is the aperture radius. The difference in the indices can be found by $\Delta n = n_c - n_s$.

Taking Δn and setting the imaginary part of the cladding's refractive index, n_s'= 0, the program calculates an initial value for the spectral splitting between the first higher-order mode and the fundamental mode. These calculated values are compared to the measured spectrum splitting, and as needed the imaginary refractive index component is increased until the calculated splitting is within a specified resolution of the measured splitting.

Loss for larger aperture devices are relatively easy to calculate, but difficulty obtaining convergence point arose for the smaller apertured VCSELs. For the smaller apertures, the initial guess for n_s' was assumed to be that obtained from the next larger device, which increased the probability of convergence of the calculations. The program output k_{01}, is then used to determine the value of the excess fundamental cavity loss.

4. Research Results

As seen in Fig 7, the current density is very large at small apertures because of the size-dependent optical loss and reduces rapidly for increasing aperture sizes. Note that broad area VCSELs have essentially constant current density which indicates no size-dependent optical loss. Based on the current density measurements in Figure 7, the transition to size-dependency is judged to be for the 7.5 µm aperture size for both samples.

Figure 11 shows the initial calculated splitting values (which assumes no imaginary refractive index component) compared to the actual measured values. For apertures smaller than 4 µm, the measured splitting is obviously greater than those from the lossless calculations. By increasing the imaginary part of the clad, the calculated splitting begins to match the measured values and the program is able to extract the loss. It is shown that for smaller apertures, the excess fundamental loss is greatest than the VCSELs with the smallest apertures, as seen in Figure 12.

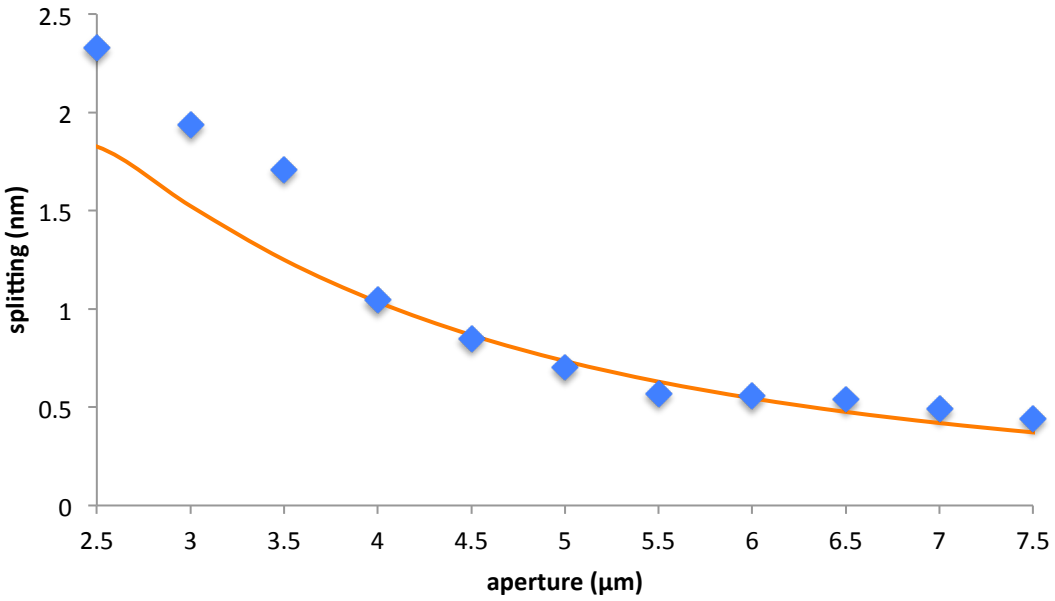

Figure 11 Initial lossless calculated values.

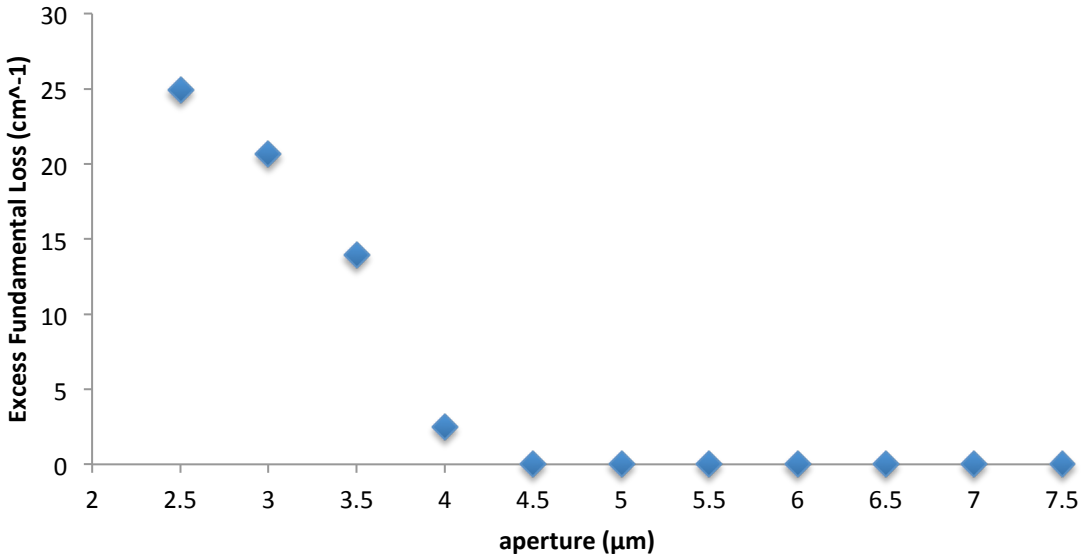

Figure 12 Fundamental excess loss obtained from matching cold-cavity spectra to program calculations.

5. Conclusion and Future Work

In this research project, by using and modifying previously determined methods, it has been demonstrated that the presence of dopants causes VCSELs to exhibit optical loss and that devices with smaller apertures have greater cavity loss than those with larger apertures. Additionally, for the samples used in this study it seems that this optical loss is sufficiently high that the differences in the doping level between the two samples is not enough to be detected. In other words, both samples show large size-dependent loss for small aperture sizes, such that the difference in doping is not detectable. However, one should be reminded that these samples were designed and grown in 1995 and that, in comparison to more recently grown epistaxis, they have a much larger optical loss.

Future work related to this project could analyze the effect of doping levels on more contemporary samples grown using newer epitaxial designs. In addition, the results of this work could be used to reduce the size-dependent loss and thus lead to improved performance for small diameter VCSELS

References

[1] K. D. Choquette, W. W. Chow, G. R. Hadley, H. Q. Hou, and K. M. Geib, "Scalability of small-aperture selectively oxidized vertical cavity lasers," *Applied Physics Letters*, vol. 70, no. 7, pp. 823-825, 1997.

[2] K. L. Lear, K. D. Choquette, R. P. Schneider, S. P. Kilcoyne, and K. M. Geib, "Selectively oxidised vertical cavity surface emitting lasers with 50% power conversion efficiency," *Electronic Letters*, vol. 31, no. 3, pp. 208-209, 1995.

[3] B. Weigl, M. Grabherr, C. Jung, R. Jager, G. Reiner, R. Michalzik, D. Sowada, and K.J. Ebeling, "High-performance oxide-confined GaAs VCSELs," *IEEE Journal of Selected Topics in Quantum Electronics*, vol. 3, no. 2, pp. 409-415, 1997.

[4] E. R. Hegblom, D. I. Babic, B. J. Thibeault, and L. A. Coldren, "Estimation of scattering losses in dielectrically apertured vertical cavity lasers," *Applied Physics Letters*, vol. 68, no. 13 pp. 1757-1759, 1996.

[5] B. J. Thibeault, E. R. Hegblom, P. D. Floyd, R. Naone, Y. Akulova, and L. A. Coldren, "Reduced optical scattering loss in vertical-cavity lasers using a thin (300 /spl Aring/) oxide aperture," *IEEE Photonics Technology Letters*, vol. 8, no. 5, pp. 593-595, 1996.

[6] C. Jung, R. Jager, M. Grabherr, P. Schnitzer, R. Michalzik, B. Weigl, S. Muller, and K. J. Ebeling, "4.8 mW singlemode oxide confined top-surface emitting vertical-cavity laser diodes," *Electronic Letters*, vol. 33, no. 21, pp. 1790-1791, 1997.

[7] R. A. Morgan, G. D. Guth, M. W. Focht, M. T. Asom, K. Kojima, L. E. Rogers, and S. E. Callis, "Transverse mode control of vertical-cavity top-surface-emitting lasers," *IEEE Photonics Technology Letters*, vol. 4, no. 4, pp. 374-377, 1993.

[8] E. W. Young, K. D. Choquette, S. L. Chuang, K. M. Geib, A. J. Fischer, and A. A. Allerman, "Single-transverse-mode vertical-cavity lasers under continuous and pulsed operation," *IEEE Photonics Technology Letters*, vol. 13, no. 9, pp. 927-929, 2001.

[9] H. Martinsson, J. A. Vukusic, M. Grabherr, R. Michalzik, R. Jager, K. J. Ebeling, and A. Larsson, "Transverse mode selection in large-area oxide-confined vertical-cavity surface-emitting lasers using a shallow surface relief," *IEEE Photonics Technology Letters*, vol. 11, no. 12, pp. 1536-1538, 1999.

[10] D. S. Song, S. H. Kim, H. G. Park, C. K. Kim, and Y. H. Lee, "Single-fundamental-mode photonic-crystal vertical-cavity surface-emitting lasers," *Applied Physics Letters*, vol. 80, no. 21, pp. 3901-3903, 2002.

[11] N. Yokouchi, A. J. Danner, and K. D. Choquette, "Two-dimensional photonic crystal confined vertical-cavity surface-emitting lasers," *IEEE Journal of Selected Topics in Quantum Electronics*, vol. 9, no. 5, pp. 1439-1445, 2003.

[12] N. Yokouchi, A. J. Danner, and K. D. Choquette, “Etching depth dependence of the effective refractive index in two-dimensional photonic-crystal-patterned vertical-cavity surface-emitting laser structures,” *Applied Physics Letters*, vol. 82, no. 9, pp. 1344-1346, 2003.

[13] A. J. Danner, J. J. Raftery,Jr., T. Kim, P. O. Leisher, A. V. Giannopoulos, and K. D. Choquette, “Progress in Photonic Crystal Vertical Cavity Lasers,” *IEICE Trans. Electron.*, vol. E88-C, no. 5, pp. 944–950, 2005.

[14] A. J. Danner, T. S. Kim, and K. D. Choquette, “Single fundamental mode photonic crystal vertical cavity laser with improved output power,” *Electronic Letters*, vol. 41, no. 6, pp. 325-326, 2005.

[15] H. Yang, F. I. Lai, H. C. Yu, C. P. Sung, H. C. Kuo, S. C. Wang, S. Y. Lin, and J. Y. Chi, “Singlemode (SMSR>40 dB) proton-implanted photonic crystal vertical-cavity surface-emitting lasers,” *Electronic Letters*, vol. 41, no. 6, pp. 326-328, 2005.

[16] A. Furukawa, S. Sasaki, M. Hoshi, A. Matsuzono, K. Moritoh, and T. Baba, “High-power single-mode vertical-cavity surface-emitting lasers with triangular holey structure,” *Applied Physics Letters*, vol. 85, pp. 5161-5163, 2004.

[17] J. H. Baek, D. S. Song, I. K. Hwang, K. H, Lee, and Y. H. Lee, “Transverse mode control by etching depth tuning in 1120-nm GaInAs/GaAs photonic crystal vertical-cavity surface-emitting lasers,” in *Conference on Lasers and Electro-Optics*, 2004, pp. 859-867.

[18] B. J. Thibeault, T. A. Strand, T. Wipiejewski, M. G. Peters, D. B. Young, S. W. Corzine, and L. A. Coldren, “Evaluating the effects of optical and carrier losses in etched‐post vertical cavity lasers,” *Journal of Applied Physics*, vol. 78, no. 10, pp. 5871-5875, 1995.

[19] T. H. Oh, D. L. Huffaker, and D. G. Deppe, “Size effects in small oxide confined vertical-cavity surface-emitting lasers,” *Applied Physics Letters*, vol. 69, no. 21, pp. 3152-3154, 1996.

[20] A. E. Siegman, “Propagating modes in gain-guided optical fibers,” *Journal of the Optical Society of America A*, vol. 20, no. 8, pp. 1617-1628, 2003.

[21] D. F. Siriani, P. O. Leisher, and K. D. Choquette, “Loss-Induced Confinement in Photonic Crystal Vertical-Cavity Surface-Emitting Lasers,” *IEEE Journal in Quantum Electronics*, vol. 45, no. 7 pp. 762-768, 2003.

[22] S. T. M. Fryslie, D. F. Siriani, and K. D. Choquette, “Cold-cavity measurements of optical loss from oxide-confined vertical-cavity surface-emitting lasers,” *Applied Physics Letters*, vol. 104, no. 10, pp. 101103 - 101103-3, 2014**.**

[23] L. A. Coldren, S. W. Corzine, and M. L. Mashanovitch, *Diode Lasers and Photonic Integrated Circuits*. Hoboken: John Wiley & Sons, Inc., 2012.

Appendix A Loss Analysis Program

The following is the MATLAB code for the loss analysis program. Green text and black text are original comments and code in the original photonic crystal loss calculations. Red text are the changes made for the purpose of oxide-confined VCSELs characterized in this study.

A.1 Edited Main Program MATLAB Code

```
% This program numerically solves the Helmholtz equation to find the
% cladding loss of a cylindrical waveguide by fitting to spectrum data

% DOMINIC SIRIANI - UNIVERSITY OF ILLINOIS - MAY 18, 2011 (final revision)
% Edited for oxide-confined loss calculations - Fall 2014
clear all;
format long;

%% Constant and variable definitions
i=sqrt(-1);
%mesa_size = 35; lambda_meas = [850.156 844.968];   %aperturesize 1.5
%mesa_size = 35.5; lambda_meas = [852.62 849.24];   %aperturesize 2.0
%mesa_size = 36; lambda_meas = [853.434 851.106];   %aperturesize 2.5
%mesa_size = 36.5; lambda_meas = [855.052 853.116];   %aperturesize 3.0
%mesa_size = 37; lambda_meas = [854.752 853.044];   %aperturesize 3.5
mesa_size = 37.5; lambda_meas = [855.38 854.336];   %aperturesize 4.0
%mesa_size = 38; lambda_meas = [855.672 854.824];   %aperturesize 4.5
%mesa_size = 38.5; lambda_meas = [855.984 855.28];   %aperturesize 5.0
%mesa_size = 39; lambda_meas = [856.108 855.54];   %aperturesize 5.5
%mesa_size = 39.5; lambda_meas = [856.406 855.848];   %aperturesize 6.0
%mesa_size = 40; lambda_meas = [856.344 855.804];   %aperturesize 6.5
%mesa_size = 40.5; lambda_meas = [856.552 856.06];   %aperturesize 7.0
%mesa_size = 41; lambda_meas = [856.524 856.08];   %aperturesize 7.5
%mesa_size = 41.5; lambda_meas = [856.654 856.226];   %aperturesize 8.0


%%%%%%%%%%%%%%%%%%%%%%%%%%%%%%%%%%%%
% Calculation Grid
% VERY IMPORTANT TO MAKE DOMAIN LARGE ENOUGH AND GRID FINE ENOUGH

%SF R=15;       % Total domain radius (increase to accommodate mode size)
R = 0.5*mesa_size;       % Total domain radius (increase to accommodate mode size)

R=15;       % Total domain radius (increase to accommodate mode size)
dr=.05;     % Grid size (decrease for better accuracy)
r=0:dr:R;   % Coordinates

% Small calculation grid (for faster gradient calculations)
% Can change to be different, but could make gradients inaccurate
% NOT RECOMMENDED TO MAKE DIFFERENT FROM OTHER GRID

R_sm=15;
%R_sm = 0.5*mesa_size;
dr_sm=.05;
r_sm=0:dr_sm:R_sm;

% Store the current directory
curdir = pwd;

% Header for output
header = {'File Name','aperture radius (nm)','b/a','depth (layers)','Delta Lambda (nm)','Delta
n','n_r Core','Veff','n_i Clad','kz','k01 (um^-1)','k11 (um^-1)'};

%fprintf('set header\n');
%% Calculate indices
% Calculate the real effective indices
[filenames,output,output_filename] = PhCVCSEL_sim((mesa_size-33.5));
```

```
%fprintf('complete PhCVCSEL_sim\n');
%% Loss calculations
% Number of files
numFiles = length(filenames);

% Get folder where data is stored and load spectrum
folder_name = uigetdir(curdir,'Select Folder Containing Spectrum Data');
%fprintf('selected spectra\n');
%% Gradient descent constants
defs = [1e-5 0.5 100 1e-6];      % Default parameters
[defs(1) defs(2) defs(3) defs(4)] = Loss_DescentPrompt(defs);    % Get user's defaults

% Perform loss calculations on all files
for fileNum=1:numFiles
    %% Set radius and clad variables
    a = output(fileNum,1)*1e-3 - 0.5*output(fileNum,2)*output(fileNum,1)*1e-3;  % Aperture radius
    ncore = output(fileNum,6);          % Core index
    nclad = ncore + output(fileNum,5);  % Cladding index
    ncimag=0;               % Core is real
    nsimag_def=0.0001;            % Imaginary part of cladding
    %fprintf('set r and clab variables\n');

    % Initialize gradient descent constants with user's defaults
    eta = defs(1);
    m = defs(2);
    maxIter = defs(3);
    tol = defs(4);
    dw = [0 0];
    %fprintf('initialize gradient descent constants\n');
%DS     %% Load the spectrum data
     cd(folder_name);
     A = importdata(int2str((mesa_size-33.5)*10),',',1); % Text file import
     %fprintf('imported spectrum data\n');
     Lg = A.data(:,1);    % Store wavelength, 1st column
     S = A.data(:,2);     % Store spectrum, 2nd column
     clear A              % Temporary variable
     cd(curdir);
%    Lg = [845 860];
    % Determine the measured resonances and splitting from the spectrum
%     lambda_meas = Loss_Peaks(Lg,S)
    split_meas = lambda_meas(1) - lambda_meas(2)
    k0 = 2*pi/(lambda_meas(1)*1e-3);
    %fprintf('set k0: %.2f\n', k0);
    %% Initial lossless guesses
    % Define the index profile
    n = ncore*ones(1,length(r));
    n(r>a) = nclad;

    % Get intial guess for kz
    % Setup the matrix
    A=diag(-2/dr^2+n.^2*k0^2)+...
        diag(1/dr^2+1./(2*r(1:end-1)*dr),1)+...
        diag(1/dr^2-1./(2*r(2:end)*dr),-1);
    % The corner elements must be treated separately to correct for r=0
    % singularity (done by assuming zero first derivative)
    A(1,1)=-4/dr^2+n(1)^2*k0^2;
    A(1,2)=4/dr^2;
    %fprintf('initial guess for kz\n');

    % Solve the eigenvalue problem
    [V,D]=eig(A);
    kzs = sqrt(diag(D));
    kzs(kzs > ncore*k0) = 0;
    kzs(kzs < nclad*k0) = 0;
    kz_def = max(kzs);   % Default starting point for kz
    %fprintf('eigenvalue problem\n');

    % Initialize kz
    kz = kz_def;

    %fprintf('start helmholtz solver\n');
```

```
% Initial lossless calculation
% Solutions to the Helmholtz equation
H = HelmholtzSolver(n,r,kz,2);
%fprintf('HelmholtzSolver\n');

% Eliminate modes not in wavelength data range
for ind1=1:length(H)
    for ind2=1:length(H(ind1).k)
        if H(ind1).k(ind2)>2*pi/(Lg(1)*1e-3) || ...
            H(ind1).k(ind2)<2*pi/(Lg(end)*1e-3)
            H(ind1).k(ind2) = Inf;
        end
    end
end

% Find the calculated peak and splitting
[M1,I1]=min(real(H(1).k));
[M2,I2]=min(real(H(2).k));
lambda_calc(1) = 2*pi/M1*1e3;
lambda_calc(2) = 2*pi/M2*1e3;

split_calc = lambda_calc(1) - lambda_calc(2)
if split_calc > split_meas
    F = 0;
else
    F = 100;
end

% Initialize nsimag
nsimag = nsimag_def;

%% Loop to iterate to desired accuracy
% Constants for terminating loop
count = 1;      % Number of iterations performed
hold off;
while F > tol
    % Define the index profile
    n = (ncore + i*ncimag)*ones(1,length(r));
    n(r>a) = nclad + i*nsimag;

    % Solutions to the Helmholtz equation
    H = HelmholtzSolver(n,r,kz,2);

    % Eliminate modes not in wavelength data range
    for ind1=1:length(H)
        for ind2=1:length(H(ind1).k)
            if H(ind1).k(ind2)>2*pi/(Lg(1)*1e-3) || ...
                    H(ind1).k(ind2)<2*pi/(Lg(end)*1e-3)
                H(ind1).k(ind2) = Inf;
            end
        end
    end

    % Find the calculated peak and splitting
    [M1,I1]=min(real(H(1).k));
    [M2,I2]=min(real(H(2).k));
    lambda_calc(1) = 2*pi/M1*1e3;
    lambda_calc(2) = 2*pi/M2*1e3;
    split_calc = lambda_calc(1) - lambda_calc(2)

    %fprintf('before loss effor\n');
    % Determine error function
    F = Loss_Error(lambda_meas(1),lambda_calc(1),split_meas,split_calc)

    % Store the maximum value of F
    if count == 1 || F > maxF
        maxF = F;
    end
    % Change the maximum value for viewing purposes
    if maxF > 10 * F
```

```
        maxF = 10 * F;
    end

    % Show how the error is changing
    figure(1);
    hFig = plot(count,F,'.k');
    axis([1 maxIter 0 maxF]);
    xlabel('Iteration Number');
    ylabel('F (Error Function)');
    title({strcat('Error for File #',num2str(fileNum)),'(Close Window to Break)'});
    drawnow;
    hold on;

    % Define the index profile on smaller grid
    n_sm = (ncore + i*ncimag)*ones(1,length(r_sm));
    n_sm(r_sm>a) = nclad + i*nsimag;

    %fprintf('before loss gradient\n');
    % Calculate gradient
    G = Loss_Gradient(n_sm,r_sm,a,kz,lambda_meas(1),split_meas);

    % Move to next point
    dw = -eta*G + m*dw;
    kz = kz + dw(1);
    nsimag = nsimag + dw(2);%%%%%%%%%%%%%%%%%%%%%%%%%%%%%%%%%%%%%%%%%%%%%%%%%%%%%%%%

    % Increment iteration count
    count = count + 1;
    %fprintf('before iteration limit check\n');
    % Check if at iteration limit and prompt user if so
    if (count > maxIter || ishandle(hFig) == 0) && F > tol
        choice = questdlg_timer(30,...
            'Max iterations reached. What would you like to do? 30 seconds to respond.',...
            strcat('Limit Reached. F = ',num2str(F)),...
            'Update Parameters','Restart','Skip','Skip');
        %fprintf('set choice\n');
        if strcmp(choice,'Restart')
            %fprintf('restart\n');
            [eta m maxIter tol] = Loss_DescentPrompt([eta m maxIter tol]);
            defs = [eta m maxIter tol];     % Since had to restart, reset defaults
            count = 1;
            hold off;
            nsimag = nsimag_def;
            kz = kz_def;
            dw = [0 0];
        elseif strcmp(choice,'Update Parameters')
            %fprintf('update parameters\n');
            [eta m incIter tol] = Loss_DescentPrompt([eta m maxIter tol]);
            maxIter = maxIter + incIter;
        else
            %fprintf('set f = 0\n');
            F = 0;
        end
    end
end

% Store solutions
% If error, set to zero. Store otherwise
if F == 0
    output(fileNum,8:11) = 0;
    %fprintf('error\n');
else
    %fprintf('storing solutions\n');
    output(fileNum,8) = nsimag;
    output(fileNum,9) = kz;
    output(fileNum,10) = H(1).k(I1);
    output(fileNum,11) = H(2).k(I2);
end
%fprintf('end\n');
% Save the field profile figures
figure(2);
```

```
    plot(r,abs(H(1).U(:,I1)).^2,r,[0; abs(H(2).U(:,I2)).^2]);
    saveas(gcf,strcat('Modes_',char('x')),'fig');

%    Save the spectrum
%    figure(2);
%    plot(Lg,S,'k',...
%       [lambda_calc(1) lambda_calc(1)],[min(S) max(S)],'--b',...
%        [lambda_calc(2) lambda_calc(2)],[min(S) max(S)],'--r');
%    saveas(gcf,strcat('Spectrum_',char(filenames(fileNum))),'fig');
    close(gcf);
end

%% Write output file
out = [filenames mat2cell(output,ones(1,size(output,1)),ones(1,size(output,2)))];
out = [header; out];
cell2csv(output_filename,out);
```

A.2 Edited PhCVCSEL.sim MATLAB Function

```
%%%%%%%%%%%%%%%%%%%%%%%%%%%%%%%%%%%%%%%%%%%%%%%%%%%%%%%%%%%%%%%%%%%%%%%%%%%%
% PhCVCSEL_sim
%
% INPUTS:
% epi_structure_filename: filename of epi structure (csv format)
% batch_filename: filename of batch param file (csv format)
% output_filename: filename of output file (csv format)
% lambda: nominal design wavelength of vcsel [nm]
% lambda_start: wavelength to start resonance search [nm]
% lambda_end: wavelength to edn resonance search [nm]
% lambda_step: wavelength step for resonance search [nm]
%
% OUTPUTS:
% output
%%%%%%%%%%%%%%%%%%%%%%%%%%%%%%%%%%%%%%%%%%%%%%%%%%%%%%%%%%%%%%%%%%%%%%%%%%%%

function [filenames,output,output_filename] = PhCVCSEL_sim(aperture_size)

x = (aperture_size*1000)/2; % Aperture radius in nm
% load epistack from file
[epistack, FileName] = LoadEpiStack;
FN = char(FileName); % convert to string
FN = FN(1:end-4); % remove .csv

% load batch params from file
[filenames,batchparams] = LoadBatchParams;

output = zeros(0);

prompt = {'Enter lambda center','Enter lambda start','Enter lambda end','Enter lambda step
size','Enter output filename (no suffix)'};
dlg_title = 'Wavelength Parameters; Output';
num_lines = 1;
def = {'850','820','880','.01',[FN,'_Output']};
answers = inputdlg(prompt,dlg_title,num_lines,def);
lambdadata=cellfun(@str2num,answers(1:4));
lambda = lambdadata(1);
lambda_start = lambdadata(2);
lambda_end = lambdadata(3);
lambda_step = lambdadata(4);
output_filename = answers(5);
output_filename = char(output_filename);
output_filename = [output_filename,'.csv'];

% convert to nstack for core
nstack = Convert_EpiStack_to_NStack(epistack, lambda);

% get reflection coeff spectrum for core
[R l] = ReflectionSpectrum(nstack, lambda_start, lambda_end, lambda_step);
```

```
% find resonance of core
l_res = MinLambda(R, 1);

% calculate ncore
[E_core z_core nz_core] = ElectricField(nstack, l_res, 1);
ncore = FieldWeightedIndex(E_core, nz_core, 1);



    dn = -(((856.524-856.080)*1e-9*ncore*(7.5)*1e-6*pi()/(856.524*1e-9*856.524*1e-
9))^2)*(2*ncore)%aperture 7.5

    % nclad
    nclad = ncore + dn;

    % Veff
    Veff = ((2*pi*x)/lambda)*(((ncore^2) - (nclad^2))^(1/2));



filenames = (aperture_size+33.5)*10;
output(1) = x;      % Aperture radius in nm
output(2) = 0;
output(3) = 0;
output(4) = 0;
output(5) = dn;
output(6) = ncore;
output(7) = Veff;

end
```